Hyperspectral reflectance signature protocol for predicting subsurface bottom reflectance in water: *in-situ* and analytical methods

Charles R. Bostater, Jr., Tyler Rotkiske, Taylor Oney

Marine Environmental Optics Laboratory and Remote Sensing Center, College of Engineering, Department of Ocean Engineering and Science, Florida Institute of Technology, 150 West University Blvd., Melbourne, Florida, USA 32901

ABSTRACT

In-situ measurement of bottom reflectance signatures & bottom features in water are used to test an analytical based irradiance model protocol. Comparisons between predicted and measured bottom reflectance signatures are obtained using measured hyperspectral remote sensing reflectance signatures, water depth and water column constituent concentrations. Analytical solutions and algorithms are used to generate synthetic signatures of different bottom types. The analytical methodology used to simulated bottom reflectance contains offset and bias that can be corrected using spectral window based corrections. Example results are demonstrated for application to coral species, submerged aquatic vegetation and a sand bottom type. Spectral windows are identified for predicting the above bottom types. Sensitivity analysis of predicted bottom reflectance signatures is conducted by varying water depth, chlorophyll, dissolved organic matter and total suspended mater concentrations. The protocol can be applied to shallow subsurface geospatial mapping using sensor based water surface reflectance based upon an analytical model solution derived from primitive radiative transfer theory.

Keywords: remote sensing, airborne image acquisition, hyperspectral remote sensing, multispectral imagery, shallow subsurface sensing, coral reef bottom reflectance, sand bottom reflectance, seagrass bottom reflectance, geospatial mapping application, water quality, sondes, bottom sediment, fluid mud, satellite imagery, fixed platform sensing.

1. INTRODUCTION

1.1 Background

Understanding radiative transfer in shallow waters is complicated by large temporal and spatial variability of the optical properties of the medium as well as the influence of bottom reflectance. This complexity necessitates the use of theoretical models both to interpret and extrapolate observational data. A mathematical reflectance model of a water body, which is based on the spectral characteristics of the water body, can connect the factors that cause a particular surface reflectance signature with the bottom signature. However, there are often trade-offs between detailed physics and computational simplicity[1].

An analytical solution to a two stream model is used to simulate bottom reflectance. The goal of the protocol approach is to specify the water surface reflectance in terms of a bidirectional reflectance factor (BRF) signature, the water depth and the water constituent properties in order to simulate a synthetic bottom reflectance signature. The numerical model used is derived from a solution to the integro-differential radiative transfer equation (RTE) described by Priesendorfer[2] applied to a water column in one spatial dimension given by:

* cbostate@fit.edu, Florida Institute of Technology, Marine Environmental Optics Lab & Remote Sensing Center, College of Engineering, Dept. Ocean Engineering and Science, 150 West University Blvd., Melbourne, Florida 32901, ph. 321-258-9134

Remote Sensing of the Ocean, Sea Ice, Coastal Waters, and Large Water Regions 2016, edited by Charles R. Bostater, Jr., Xavier Neyt, Caroline Nichol, Oscar Aldred, Proc. of SPIE Vol. 9999, 99990N · © 2016 SPIE · CCC code: 0277-786X/16/$18 · doi: 10.1117/12.2241547

Downloaded From: http://proceedings.spiedigitallibrary.org/ on 04/05/2017 Terms of Use: http://spiedigitallibrary.org/ss/termsofuse.aspx

$$\cos\theta \frac{dL(\theta,\phi,z,\lambda)}{dz} = -c_{tc}(z,\lambda)L(\theta,\phi,z,\lambda) + \int_{\phi=0}^{2\pi}\int_{\theta=0}^{\pi} \beta(\theta',\theta,\phi',\phi,z,\lambda)L(\theta',\phi',z,\lambda)\sin\theta' d\theta' d\phi' + \beta(\theta_s,\theta,\phi_s,\phi,z,\lambda)L_s(\theta_s,\phi_s,z,\lambda), \quad (\mathrm{Wm^{-3}sr^{-1}}) \tag{1}$$

where z=water depth, positive downward, z=0 at the surface (m), $c_{tc}(z)$=total beam attenuation coefficient (m^{-1}), $\beta(\theta',\theta,\phi',\phi,z,\lambda)$ = volume scattering function of diffused radiance (m^{-1} sr^{-1}), $\beta(\theta_s,\theta,\phi_s,\phi,z,\lambda)$ =volume scattering function of collimated radiance (m^{-1} sr^{-1}), $L(\theta_s,\phi_s,z,\lambda)$ =collimated radiance (W m^{-2} sr^{-1}), θ_s, ϕ_s =solar zenith angle (θ_s) and solar azimuth angle (ϕ_s) (radians), λ =wavelength of light.

Solutions to the above require simplification in order to simulate fast and accurate estimates of the light distribution in a water column. The analytical solution used is based upon the two-flow equation solutions developed and advanced by Bostater et al, 1995[3] for Case I and Case II models and Bostater and Huddleston, 2006[4]. The method of solution can be applied any one of many versions of the two-stream model, with or without the inclusion of shape factors. Synthetic bottom reflectance signatures in this paper are produced using the solution given by Bostater et al., 1995[3]. The radiative transfer equation solutions allows the simulation of the direct and indirect irradiant light fields according to the two-flow equations that may include shape factors and can be written as[4]:

$$\frac{dE_d(z)}{dz} = -(a_d + b_d)E_d(z) + b_u E_u(z) + cE_s(z), \tag{2}$$

$$\frac{dE_u(z)}{dz} = (a_u + b_u)E_u(z) - b_d E_d(z) - cE_s(z), \tag{3}$$

$$\frac{dE_s(z)}{dz} = -\alpha E_s(z). \tag{4}$$

where $a_d = \frac{a}{\mu_d}$, $a_u = \frac{a}{\mu_u}$, $b_d = \frac{r_d b}{\mu_d}$, and $b_u = \frac{r_u b}{\mu_u}$. These coefficients are the downwelling diffuse absorption coefficient, upwelling diffuse absorption (a) coefficient, downwelling diffuse backscattering (b) coefficients respectively[5,6,7,8]. The downwelling and upwelling shape factors, r_d and r_u, - the normalized contributions to the downwelling or upwelling radiance backscatter coefficient from the scattering lobe of the water or hydrosol volume scattering function[6]. Simplification to a form without the particular solution (homogeneous) by using only equations (2) and (3) above, for nadir viewing geometry and setting c=0 in the upwelling and downwelling equations produces the Case I solution[3] for the surface reflectance factor (BRF) in a water column with depth h, at or near the water surface or:

$$R_s(0) = \frac{R_b(h)\left(\frac{X^2}{4} - \frac{XYa}{2\varphi} - \frac{XYb}{2\varphi} + \frac{Y^2a^2}{4\varphi^2} + \frac{Y^2ab}{2\varphi^2} + \frac{Y^2b^2}{4\varphi^2}\right) + \frac{XYb}{4\varphi} - \frac{Y^2ab}{4\varphi^2} - \frac{Y^2b^2}{4\varphi^2}}{1 - \frac{R_b(h)Yb}{4\varphi^2}(\varphi X - Ya - Yb) - \frac{Y^2b^2}{4\varphi^2}} \tag{5},$$

where:

$$X = e^{\varphi h} + e^{-\varphi h},$$
$$Y = e^{\varphi h} - e^{-\varphi h},$$
$$\varphi = \sqrt{a^2 + 2ab},$$
$$a = a_{h20} + a^*_{chl}c_{chl} + a^*_{DOM}c_{DOM} + a^*_{SM}c_{SM},$$
$$b = b_{h20} + b^*_{chl}c_{chl} + b^*_{SM}c_{SM}.$$

The a's and b's can be assumed to be applicable to pure natural water conditions (h_20) and waters with chlorophyll pigments (chl-a), dissolved organic matter (DOM) and total suspended matter or seston (SM) concentrations.

Downloaded From: http://proceedings.spiedigitallibrary.org/ on 04/05/2017 Terms of Use: http://spiedigitallibrary.org/ss/termsofuse.aspx

Equation[3] 5 can then be solved for the bottom reflectance factor or $R_b(h)$ at the bottom depth - h. All terms in the above are a function of wavelength λ except the concentrations C_{DOM}, C_{SM}, and C_{chl} and depth h. The bottom reflectance factor $R_b(h,\lambda)$ for nadir viewing geometry can then be shown to be:

$$Rb(h,\lambda) = \frac{(\frac{XYb}{4\varphi} - \frac{Y^2ab}{4\varphi^2} - \frac{Y^2b^2}{4\varphi^2}) - R_s(1 - \frac{Y^2b^2}{4\varphi^2})}{-R_s(\frac{Yb}{4\varphi^2}(\varphi X - Ya - Yb)) - (\frac{X^2}{4} - \frac{XYa}{2\varphi} - \frac{XYb}{2\varphi} + \frac{Y^2a^2}{4\varphi^2} + \frac{Y^2ab}{2\varphi^2} + \frac{Y^2b^2}{4\varphi^2})} \quad (6)$$

The above analytical solution for bottom reflectance signature can be used to generate synthetic bottom reflectance spectrums as outlined in the protocol method described in the next section of this paper when a remotely sensing surface reflectance R_s is specified, for example from a hyperspectral image.

The importance of quantitative understanding the full analytical solution to equation 1 and reduced to 6 can be qualitatively appreciated and demonstrated by examining shallow imagery and the desire to discriminate and estimate different bottom types and features (sand, mud, submerged aquatic vegetation and corals, etc.) in a water body.

For example, Figure 1 shows six different shallow water images acquired from different remote sensing platforms and different imaging system configurations. Figure 1 (a) was acquired at ~1000 m using a high definition video camera mounted in a Cessna 414, and shows submerged vegetative features in shallow waters near Wabasso, Florida during Jan, 2015. Figure 1(b) is a WorldView 3 satellite image of Indian River Lagoon in Melbourne, Florida and the nearby coastal waters. This image shows the presence of subsurface and bottom reflectance effects at the water surface in a turbid estuarine lagoon and nearby coastal waters. Figure 1(c) shows the presence of submerged coral reef bottom reflectance observed in in clear waters within the Abaco Islands and mixed sand & reef features within a marine sanctuary near Scotland Cay and Man of War Cay, Bahamas. Figure 1(d) is a high spatial resolution scanned aerial image of submerged vegetation and sand bottom reflectance showing prop scars after the Deepwater Horizon oil spill incident along Florida's Panhandle region at Okaloosa Island within Choctawhatchee Bay, Florida. The image was acquired in March 11, 2011 at a 1200 m altitude using AGFA AVIPHOT Color X400 PE1 color negative high speed film and a K17 Fairchild camera. Figure 1(e) shows the presence of subsurface bottom reflectance within waters from a hyperspectral image and nearby wetland areas acquired March 12, 2011 and reported in Bostater, 2012[10]. Figure 1(f) is an airborne HD color digital image of Palm Bay Florida acquired February, 2015 and enhanced to show subsurface bottom features in a coastal turbid waters with muck and a *fluid mud bottom type*. The image was collected at ~500 m from a twin engine Cessna 414 prior to dredging of the water body. The GSD of the RGB image is ~3 cm and suggests changes in the subsurface mud and mixed bottom reflectance in this turbid shallow waterbody.

The images underscores the fact that analysis of surface water reflectance of shallow water types require the use of analytically based remote sensing algorithms that are (1) scientifically based upon radiative transfer theory, (2) that quantitatively account for variable water depth, and (3) constituent concentrations within the water column in order to interpret the imagery in order to develop water quality related algorithms. The protocol method described below demonstrate how to utilize surface reflectance in order to simulate bottom reflectance types for developing algorithms for mapping bottom features within optically shallow coastal waters.

2. TECHNIQUES & METHODS

2.1 Synthetic Bottom Reflectance Signature Simulations

Equation 5 is used to demonstrate the validity of the analytical description of bottom reflectance. In order to test and demonstrate the solution, pure water absorption and backscatter spectrums are specified - a(λ) and b(λ) as reported in Bostater, Gimond and Campbell, 2000[11] and Smith and Baker, 19841[12]. *In-situ* bottom reflectance (BRF) signatures collected by Bostater, 1997[13] in clear coastal water are utilized in the synthetic simulation process to obtain the associated clear sky irradiance reflectance signatures at or near the water surface using equation 3. Figures 2 and 3 show the spectral signatures used in the simulation process. Figure 4 shows the instrumentation developed in the Marine and Environmental Optics Laboratory used to collect specific absorption and specific the backscatter coefficients for SE US coastal water stations. Figure 3 also shows specific absorption and backscatter coefficients for clear natural water, and bottom reflectance spectrums collected with the custom underwater spectrograph in Figure 4 (right).

Downloaded From: http://proceedings.spiedigitallibrary.org/ on 04/05/2017 Terms of Use: http://spiedigitallibrary.org/ss/termsofuse.aspx

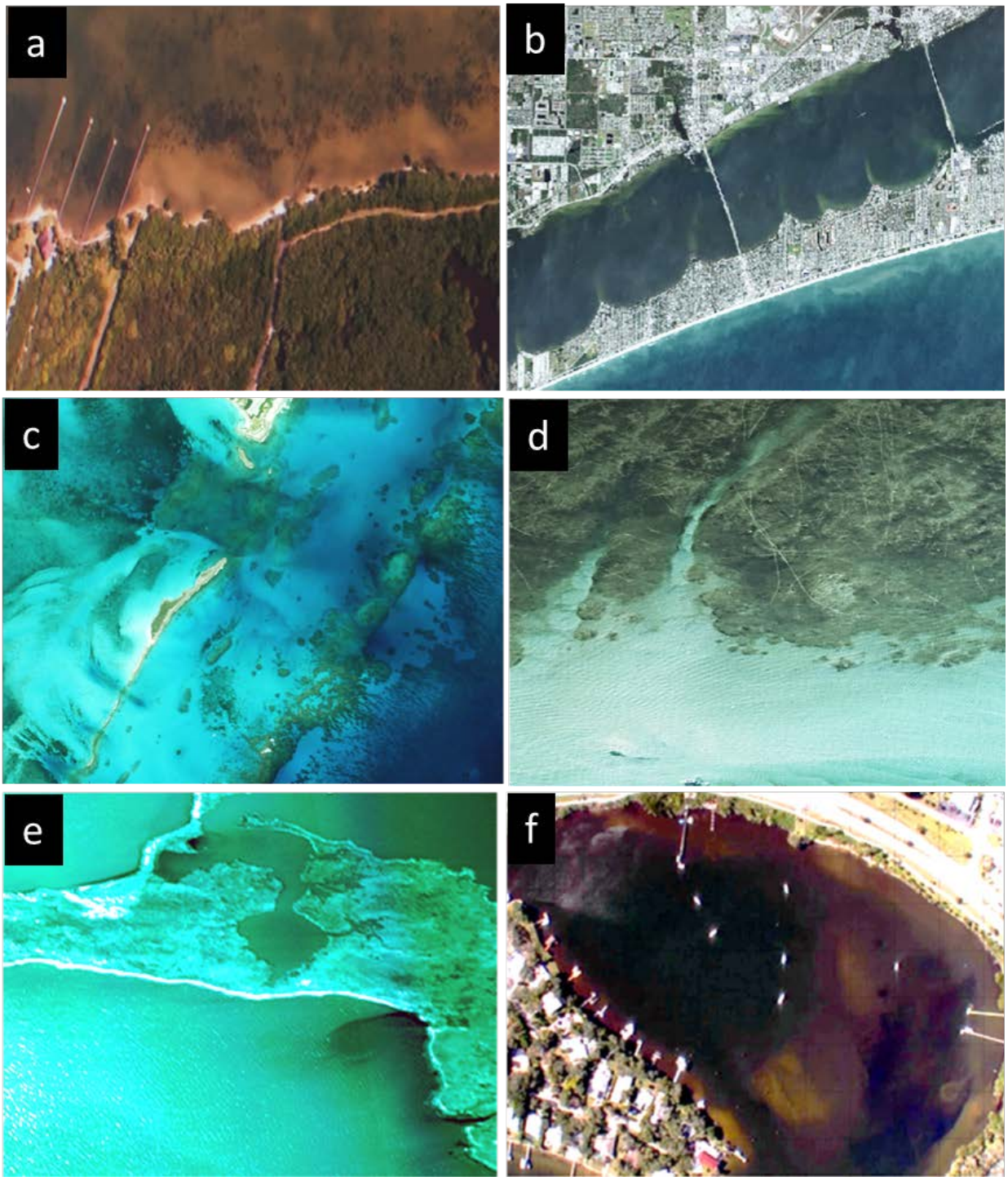

Figure 1. Imagery influenced by bottom reflectance effects. Upper left (a) high definition multispectral 3 band image showing submerged grasses (SAV) and benthic algae. Image (b) WorldView 3 satellite image of Indian River Lagoon, Melbourne, & Palm Bay Florida using the coastal color bands. Middle left (c) satellite image (WorldView 3) of a coastal coral reef marine sanctuary, Abaco Islands, Bahamas. Figure (d) is a scanned photogrammetric image show prop scars in shallow SAV waters along the Florida Panhandle region. The lower left hyperspectral image (e) shows shallow waters influenced by subsurface oil. Figure (f) shows the turbid Palm Bay, Florida estuary with a muck, fluid mud and sand mixed bottom.

Downloaded From: http://proceedings.spiedigitallibrary.org/ on 04/05/2017 Terms of Use: http://spiedigitallibrary.org/ss/termsofuse.aspx

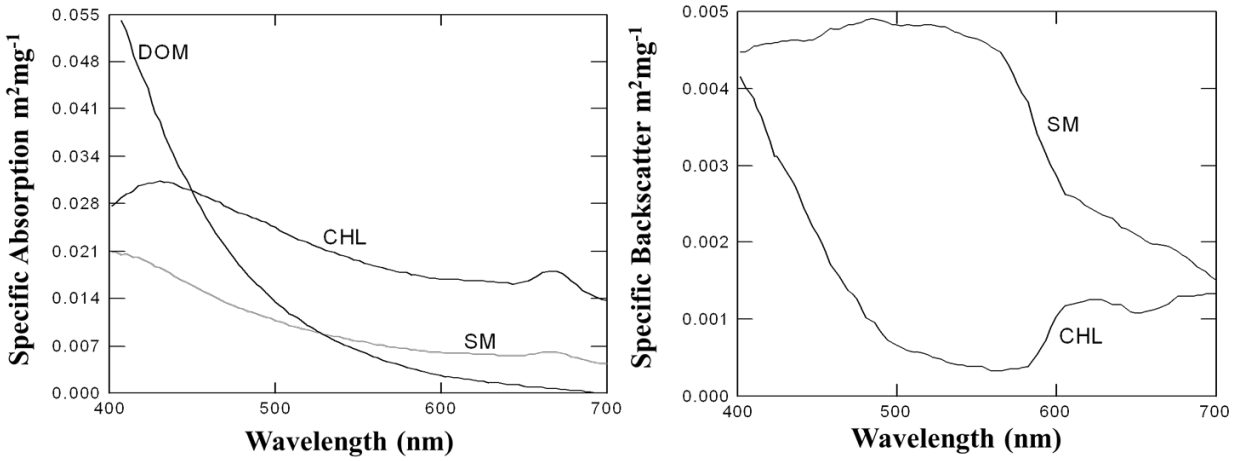

Figure 2. Spectrums of specific absorption (left) coefficients (m^2 mg^{-1}) for dissolved organic (DOM), chlorophyll-a (CHL) and seston or total suspended matter (SM) obtained from a long a pathlength cuvette for south eastern US coastal waters. Specific backscatter coefficients (m^2 mg^{-1}) for seston and chlorophyll-a (m^2 mg^{-1}) calculated using the same station *in-situ* data and surface reflectance (BRF) spectrums. Spectrums data are used in development of synthetic reflectance (BRF) of different bottom types and water depths.

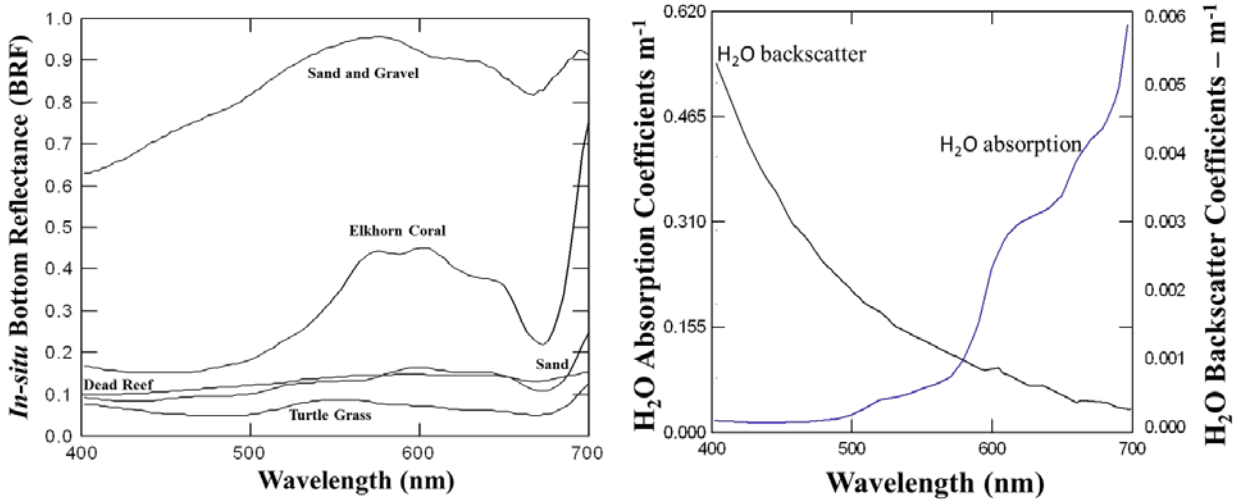

Figure 3. Spectrums (right) of clear natural water absorption (left) coefficients (m^{-1}) from Smith and Baker, 1984[12] and backscatter coefficients (m^1) for clear natural water[14] obtained from a long a pathlength cuvette. *In-situ* bottom reflectance (BRF) spectrums (left) for various bottom types measured[13] with a custom underwater SE590 high sensitivity spectrograph.

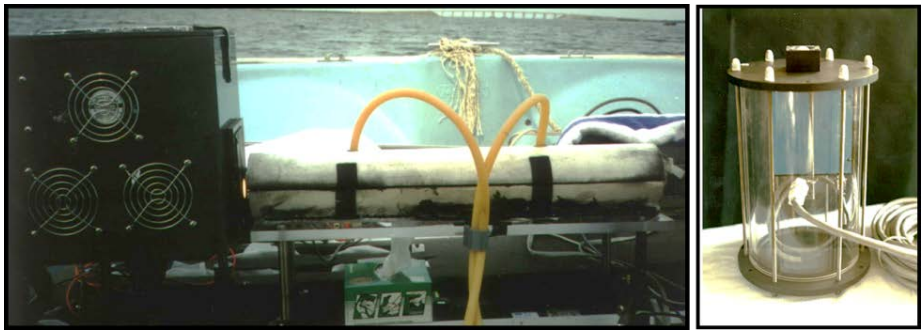

Figure 4. Shipboard long pathlength cuvette used to collect *in-situ* absorption spectrums (left) from continuously pumped water. *In-situ* submersible spectrograph (right) for collecting bottom reflectance signatures (BRF's) of bottom types used in equation 6.

Downloaded From: http://proceedings.spiedigitallibrary.org/ on 04/05/2017 Terms of Use: http://spiedigitallibrary.org/ss/termsofuse.aspx

Specific coefficients shown in Figure 2 for water constituents were determined using the long pathlength cuvette *in-situ* with continuously pumped or within the lab by using collected water samples[14]. Figure 3 shows measured nadir viewing BRF bottom reflectance signatures collected with the submersible spectrograph (Spectron SE590). Figure 3 also shows the spectral signatures of clear water absorption[12] and the calculated clear natural water backscatter signature using the method described in Bostater et al., 1995[3,11,13].

The computational process allows one to obtain simulated bottom type reflectance signatures in clear natural waters by varying the water depth (h) using equation 6 and the input spectrums shown in Figures 2 and 3 above. The simulation methodology using equation 6 can also be used when using collected *in-situ* attenuation coefficient spectrums[15] k(λ) in order to calculate b(λ) using the methodology described by Bostater and Klemas, 1988[15]. For example an attenuation signature for water in Palm Bay, Florida was obtained a submerged spectrograph in August, 2016 after recent dredging operations. The reflectance data and equations shown in Figure 5 in Bostater and Klemas[15] allows a second method for calculation of both the backscatter spectrum and the attenuation characteristics (K/K_{max}) for different estuarine water areas as demonstrated by Bostater[15] for fourteen different coastal and estuarine areas from Cape Cod to the Neuse River estuary, NC. Figure 5 shows the Palm Bay attenuation spectrum that is characteristic of Indian River Lagoon turbid waters with high concentrations of dissolved organic matter, gelbstoff and shallow fluid muds. The maximum light penetration coincides with the spectral window of minimum photosynthesis rate[16].

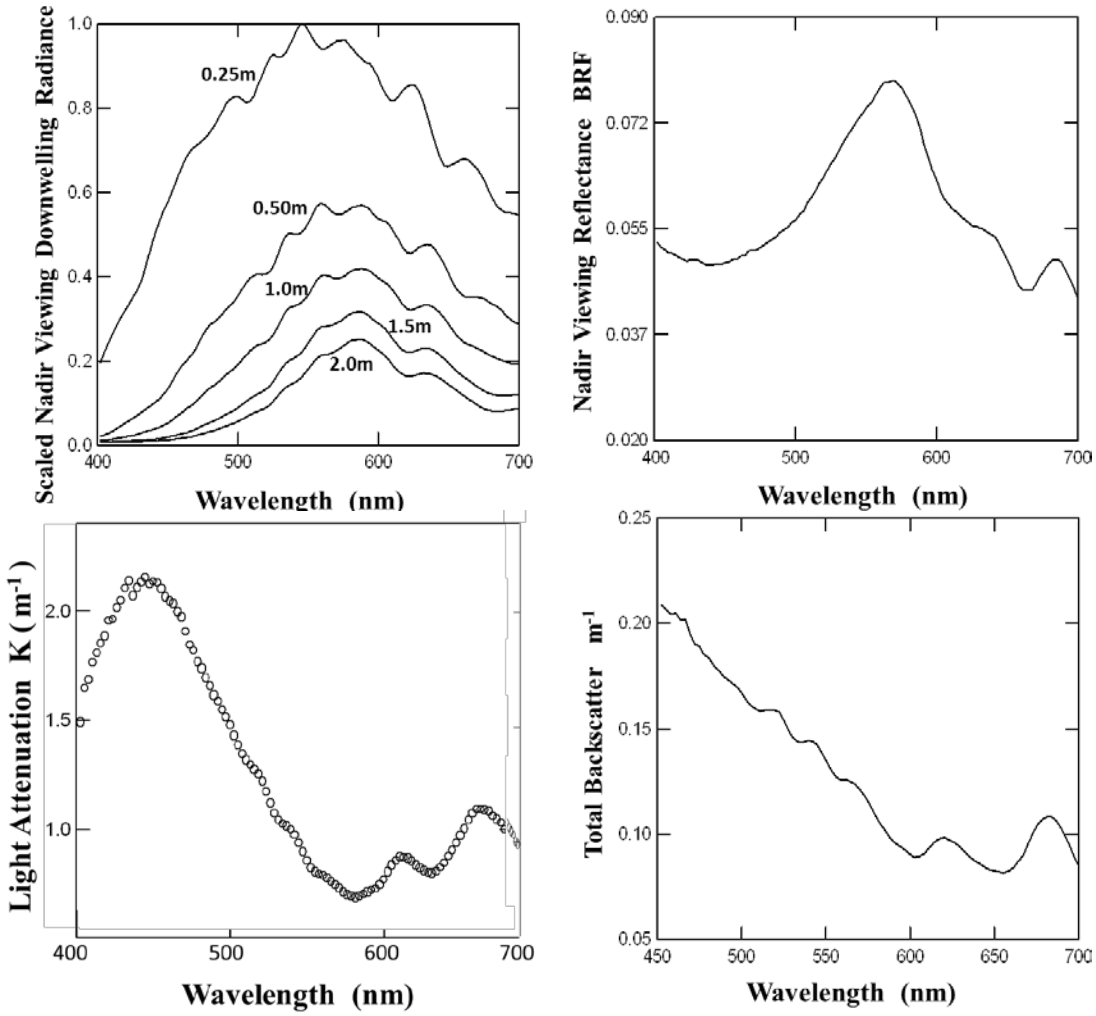

Figure 5. Calculated shipboard *in-situ* optical (left) attenuation (k – m^{-1}) signature of Palm Bay, Florida water during August, 2016 indicating the maximum depth penetration of light is 570-590 nm (yellow) in this shallow Indian River Lagoon turbid water type using depth dependent spectral measurements of light penetration[15] (right) from 0.25-2m depths. Scaled nadir viewing radiance used to calculate k(λ) and the total backscatter calculated from the reflectance and attenuation spectrums[15].

Downloaded From: http://proceedings.spiedigitallibrary.org/ on 04/05/2017 Terms of Use: http://spiedigitallibrary.org/ss/termsofuse.aspx

The procedure used to solve the two stream differential equations models[3,4] and used in Monte-Carlo modeling comparisons[9] utilizes boundary conditions(BC's) specifying and E_d and $d(E_d)/dz$ at the water surface and E_u and $d(E_u)/dz$ and the bottom when solving for the decoupled forms of equations 1 and 2 given above., or in the homogeneous forms of these equations[3]. The Cauchy type BC'scan be specified in numerous ways[3] and one method is to account for the change in $d(E_u)/dz$ through direct measurements of water constituents as a function of depth within the bottom boundary layer.

Using *in-situ* sondes described by Bostater and Rotkiske, 2015[17,18,19] in the form of a vertical array of sondes shown below (right) provides another method to describe the exponential form of the decay of light bottom light fields through analysis of water quality samples collected at or near the bottom. Figure 6 shows results from sondes that are deployed in the bottom boundary layer to collect the horizontal particulate fluxes of seston and fluid mud. As can be seen, the sondes can provide the necessary boundary condition formulations that can be used in soft mud or estuary bottom types. This advancement due to this new sampling method and protocol allows one to determine the effects of the vertical bottom boundary fluid mud profiles upon the underwater light field at or near the bottom boundary.

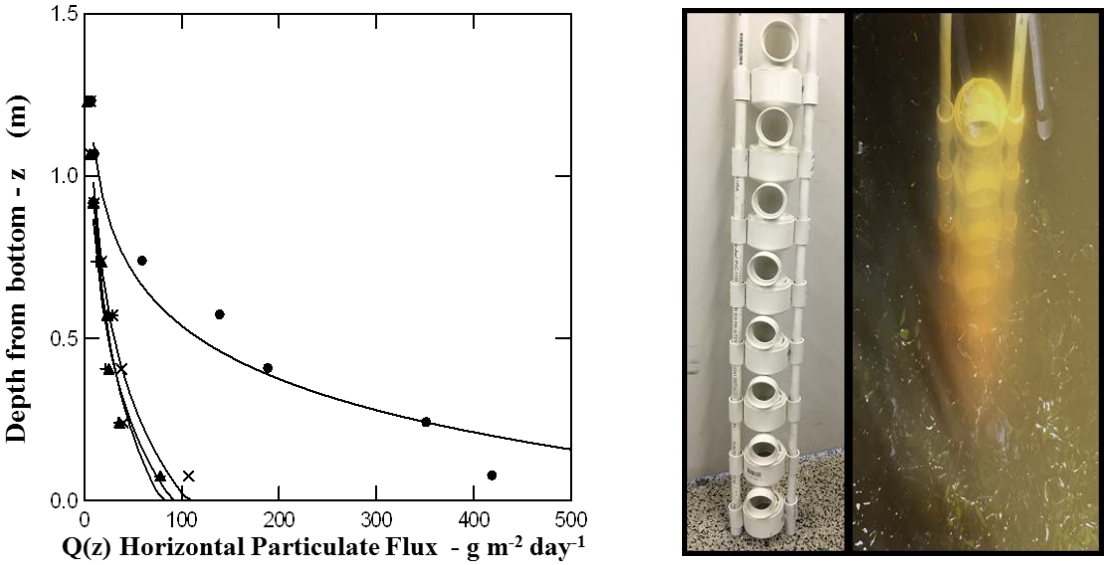

Figure 6. *In-situ* bottom boundary layer suspended sediment (fluid mud) dry weight measurements (left) made within the lower 1.25 meter water column depth at Palm Bay, Florida during 4 deployment periods during July and August, 2016. Note the several orders of magnitude sediment increase near the bottom compared to values within the free flowing upper water column depth near 1 m. The water column particulates significantly influences the bottom boundary condition light field attenuation or $d(E_u)/dz$ and $d(E_d)/dz$ at the bottom (h=0). The influence upon the light field and the mass concentrations shown are obtained from utilizing the vertical array of sondes shown in figure (right) above.

The horizontal flux as a function of depth shown in Figure 6 (left) is modeled using a time dependent or a steady state (SS) form of Burgers equation. A form of the ordinary differential equation where Q(z) has units of g m^{-2} t^{-1} or flux density, k_1 is an inverse velocity scale –T/L and k_2 is an inverse dispersion coefficient – T/L^2, respectively. The overbars denote averaged values obtained during the deployment time of the sondes. The steady state scale can vary from hours to a few days.

$$\frac{d\,\overline{Q(z)}}{dt} = \overline{k}_1 \frac{\partial \overline{Q(z)}}{\partial z} - \overline{k}_2 \frac{\partial^2 \overline{Q(z)}}{\partial z^2} \qquad (7).$$

A solution of the SS form of the above ordinary differential equation (ODE) gives the exponential form of the horizontal fluxes of particles in the bottom boundary layer (similar to the light field decay in this part of the water column) as shown in Figure 6 above is be shown to be:

$$Q(z) = Q_h \exp\left[-\frac{k_1}{k_2} z \right] \qquad (8).$$

Downloaded From: http://proceedings.spiedigitallibrary.org/ on 04/05/2017 Terms of Use: http://spiedigitallibrary.org/ss/termsofuse.aspx

The constants can be determined by linearizing the above and performing a bet fit using a general linear model (GLM) estimation procedure and matching to the light field rate of change in the same depth regime. During August, 2016 a hyperspectral image was collected of the Palm Bay turbid bottom and waters and is shown in Figure 7.

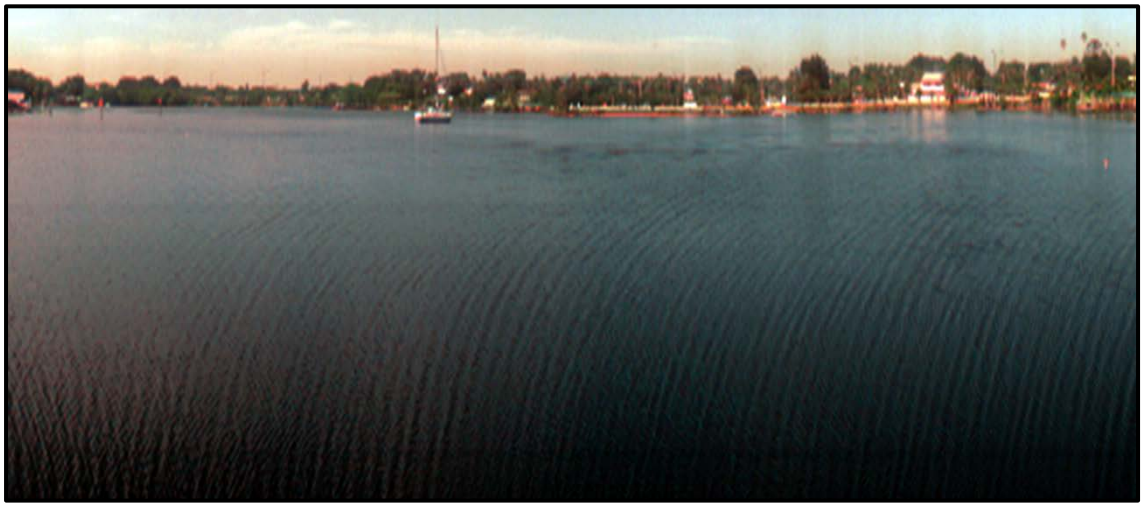

Figure 7. Palm Bay hyperspectral image 3 band snapshot collected August, 2016. Surface and in-situ data was collected near the vessel shown in the image. Image was acquired from a fixed platform near the mouth of the sub-estuary of Indian River Lagoon, Florida. The water surface reflectance at the *in-situ* station area is shown in Figure 5. The image was collected using the HSI imaging system and a rotation stage described by Bostater[10].

3. RESULTS AND DISCUSSION

Using the data, methods and procedures described in the Section 2 above, equation 6 was used to simulate the water surface reflectance. Resulting synthetic bottom reflectance (BRF) signatures for nadir viewing geometry are produced for clear natural waters (a) from 1 to 15 m depth. Note the spectral window 440 to 560 nm. Signatures are then shown for results within a 95% confidence interval of observed bottom reflectance for a Elkhorn coral bottom type.

Synthetic bottom signatures in (c) and (d) show the influence of dissolved organic matter - DOM (13.1 μg m^{-3}), seston - SM (9.2 μg m^{-3}), and chlorophyll-a CHL (1.2 μg/m^{-3}) by specifying concentrations. Simulated bottom reflectance's down to a 5m water depth are simulated and shown in Figure 8 for an **Elkhorn coral bottom type**. The spectral window (d) suggests a unique spectral window (520-560 nm) within 95% confidence of the observed bottom reflectance where a remote sensing algorithm is applied to detect live coral type based upon surface water BRF reflectance.

Figure 9 shows synthetic bottom reflectance (BRF) signatures for nadir viewing geometry for a seagrass species. The influence of water depth in clear natural water (a) from 1 to 15 m water depth. Also note an associated spectral window from 440-560 nm (b) where simulated bottom signatures are within 95% confidence interval of observed bottom reflectance for the ***Turtle grass bottom type***. The synthetic bottom signatures (c) and (d) show the influence of dissolved organic matter - DOM (13.1 μg/m-3), seston - SM (9.2 μg/m-3), and chlorophyll-a CHL (1.2 μg/m-3) when the specified concentrations effects the simulated bottom reflectance to a 5 m water depth. Again, note a unique spectral (d) window (510-560 nm) within 95% confidence of observed bottom reflectance where a remote sensing algorithm could be used to detect a submerged seagrass bottom type.

Downloaded From: http://proceedings.spiedigitallibrary.org/ on 04/05/2017 Terms of Use: http://spiedigitallibrary.org/ss/termsofuse.aspx

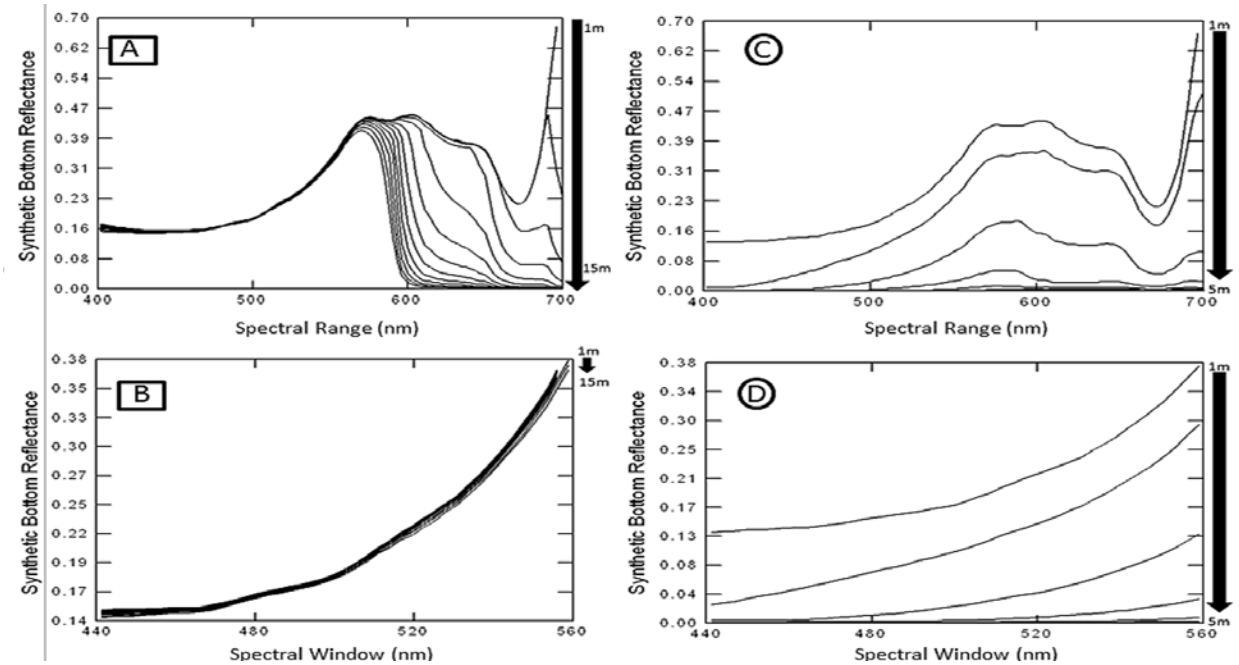

Figure 8. Synthetic bottom reflectance (BRF) signatures for nadir viewing geometry. (a) The effect of water depth in clear water (a) from 1-15 m depth. Note an associated spectral window 440-560 nm (b) where simulated bottom signatures are within 95% confidence interval of observed bottom reflectance for ***Elkhorn coral bottom type***. Synthetic signatures (c) and (d) show the influence of dissolved organic matter DOM (13.1 μg/m-3), seston SM (9.2 μg/m-3), and chlorophyll-a CHL (1.2 μg/m-3) specified concentrations effects upon bottom reflectance to a 5 m water depth. (d) Suggests a unique spectral window (520-560 nm) within 95% confidence of an observed bottom reflectance where a remote sensing algorithm[20] could be used to detect live coral types.

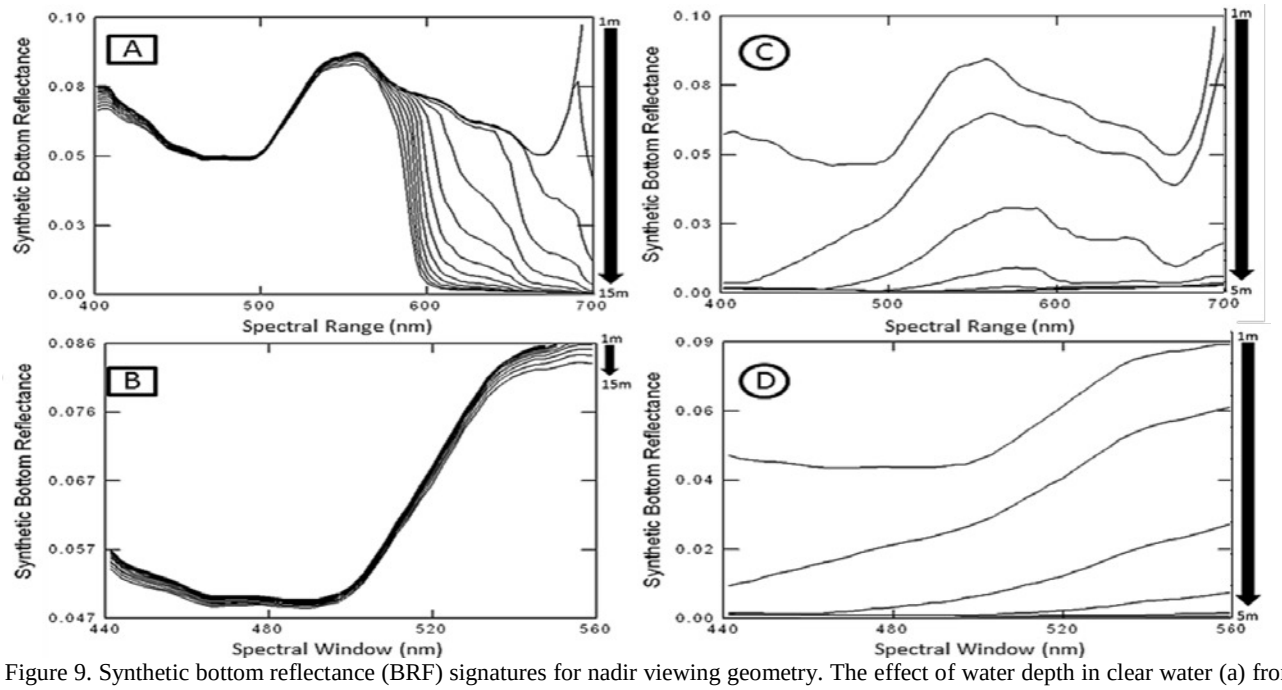

Figure 9. Synthetic bottom reflectance (BRF) signatures for nadir viewing geometry. The effect of water depth in clear water (a) from 1 to 15 m depth. Note an associated spectral window 440-560 nm (b) where simulated bottom signatures are within 95% confidence interval of observed bottom reflectance for ***Turtle grass bottom type***. Synthetic signatures (c) and (d) show the influence of dissolved organic matter DOM (13.1 μg/m-3), seston SM (9.2 μg/m-3), and chlorophyll-a CHL (1.2 μg/m-3) specified concentrations effects upon simulated bottom reflectance to a 5 m water depth. A unique spectral (d) window (510-560 nm) within 95% confidence of observed bottom reflectance can be used to develop an algorithm to detect a submerged seagrass bottom type[20].

Downloaded From: http://proceedings.spiedigitallibrary.org/ on 04/05/2017 Terms of Use: http://spiedigitallibrary.org/ss/termsofuse.aspx

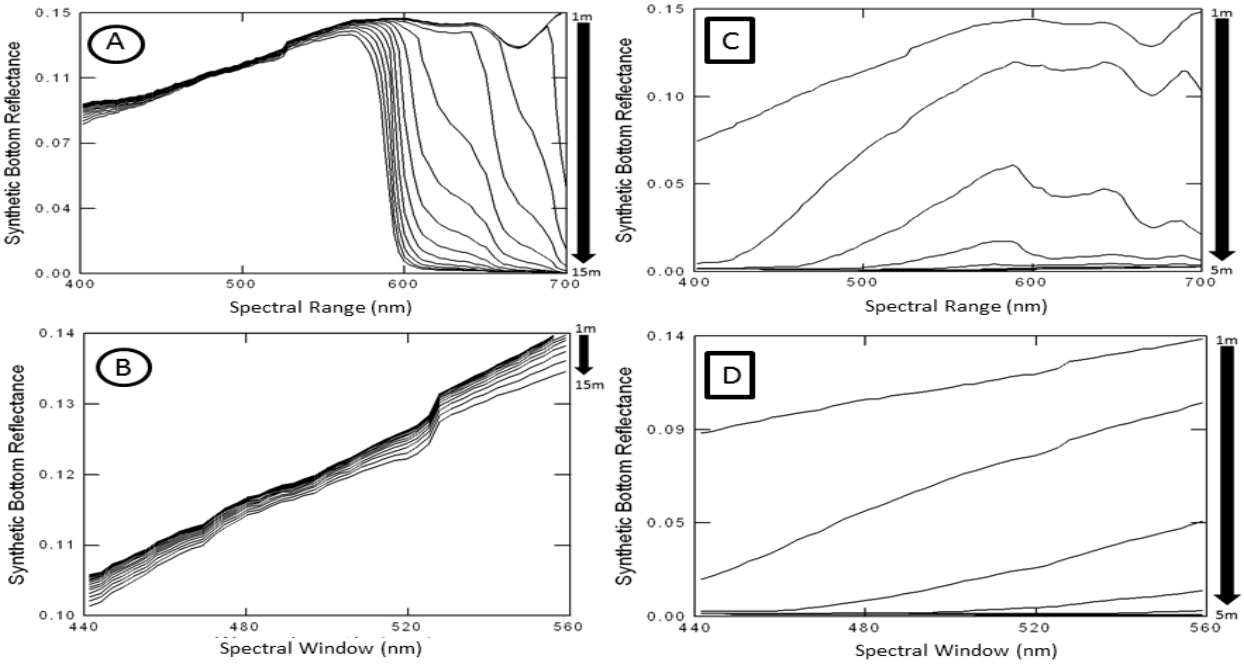

Figure 10. Synthetic bottom reflectance (BRF) signatures for nadir viewing geometry. The effect of water depth in clear water (a) from 1-15 m depth. Note an associated spectral window 440-560 nm (b) where simulated bottom signatures are within 95% confidence interval of observed bottom reflectance for a ***sand bottom type***. Synthetic signatures (c) and (d) show the influence of dissolved organic matter DOM (13.1 µg/m-3), seston SM (9.2 µg/m-3), and chlorophyll-a CHL (1.2 µg/m-3) specified concentrations effects upon simulated bottom reflectance to a 5 m water depth. A unique spectral (d) window (510-560 nm) within 95% confidence of observed bottom reflectance where a remote sensing algorithm[20] could be used to detect a sand bottom type.

Similar results for other bottom types shown in Figure 3 and simulations shown in Figure 10 have been obtained. The protocol allows one to utilize a characteristic bottom reflectance followed by using sensor derived surface water BRF signatures obtained from an airborne hyperspectral system, a high digital and radiometric sensitivity satellite system or from a vessel in order to map bottom types. The resulting synthetic signatures then form the basis for algorithms making use of the spectral windows and derivative spectroscopy[20].

Figure 11 shows an example of observed versus measured BRF bottom reflectance comparison for a 4 meter water column with constituent concentrations. The higher reflectance's at two channels near 0.14 and 0.17 suggests that at 4 meters there is reflectance deviation at only 2-3 channels.

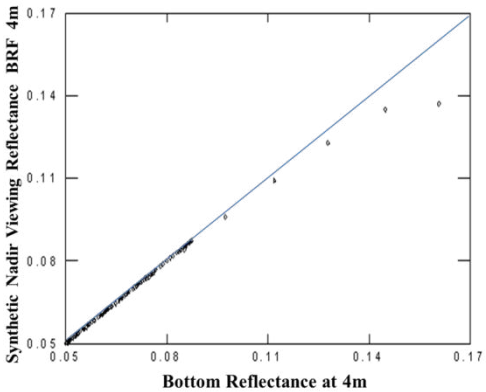

Figure 10 Turtle grass synthetic simulation versus bottom reflectance in water at 4 m water depth for 255 hyperspectral channels indicating the modeling approach provides agreement between measured and simulated bottom reflectance in clear water types.

Downloaded From: http://proceedings.spiedigitallibrary.org/ on 04/05/2017 Terms of Use: http://spiedigitallibrary.org/ss/termsofuse.aspx

4. SUMMARY AND CONCLUSIONS

The purpose of this paper has been to report on the development and testing of an analytical hyperspectral modeling protocol that utilizes measured surface hyperspectral imaging surface reflectance's to predict bottom reflectance in clear water types and waters with constituent concentrations. The paper has presented an analytical solution to the two flow model equations that predict bottom reflectance. The paper described the sensing systems and data used for use in shallow littoral zone environmental monitoring and surveillance. High spatial and spectral resolution images presented in this paper are examples of satellite, airborne, vessel and fixed platform spectral imaging technology available for characterization of the water surface as well as subsurface bottom features in aquatic systems. The integrated hyperspectral sensor systems (fixed and *in-situ*) and data reported above are examples of sensor integrations for shallow water remote sensing research. The protocol presented and method to evaluate bottom reflectance types has potential application to geospatial subsurface feature analysis and related vegetation dysfunction.

5. ACKNOWLEDGEMENTS

The development and integration of the imaging systems and software reported in this work have been developed with funding from KB Science. Research and students in the laboratory have been supported in part by the Northrop Grumman Corporation, NASA, Kennedy Space Center, the National Science Foundation, the *US-Canadian Fulbright Program*, the US Department of Education, ***FIPSE*** & European Union's grant ***Atlantis STARS*** **(Sensing Technology and Robotics Systems)** to Florida Institute of Technology, the Budapest University of Engineering and Economics (BME) and the Belgium Royal Military Academy, Brussels Acknowledgement is also given for funding for lab and student support from the Florida Dept. of Environmental Protection and Brevard County, Florida. A special acknowledgement is given to Andre Bassette at United Space Coast Cables, Melbourne, Florida, for assisting with the underwater spectrograph cable connection.

6. REFERENCES

[1] Perovich, D. K,. "A two-stream multilayer, spectral radiative transfer model for sea ice", U.S. Army Cold Regions Research and Engineering Laboratory, CRREL, Report 89-15, NTIS, 24 pp. (1989)
[2] Preisendorfer, R., *Hydrologic Optics*, Honolulu, HI, NOAA/ERL (1978)
[3] Bostater, C., W. Ma, T. McNally, M. Gimond, and A. P. Lamb, "Application of an optical remote sensing model", SPIE Vol. 2586, pp. 32-43 (1995)
[4] Huddleston, L., Bostater, C., "A sensitivity Analysis of Irradiance Reflectance Calculated From The Modified Two-Flow Equations With Shape Factors to Various Model Inputs", SPIE Vol. 6360, pp. 63600J1-19 (2006)
[5] Aas, E., "Two-stream irradiance model for deep waters", Applied Optics **26**(11): 2095-2101 (1987)
[6] Stavn, R. H. and A. D. Weidemann, "Shape factors, two-flow models, and the problem of irradiance inversion in estimating optical parameters", Limnology and Oceanography 34: 1426-1441 (1989)
[7] McCormick, N. J. and P. W. Francisco, "Radiative transfer two-stream shape factors for ocean optics", Applied Optics 34(27): 6248-6255 (1995)
[8] Hojerslev, N. K.,"Analytic remote-sensing optical algorithms requiring simple and practical field parameter inputs", Applied Optics 40(27): 4870-4874 (2001)
[9] Gimond, M. (2005). "Comprehensive assessment of the two-flow model's shape factors in aquatic environments", Applied Optics 44(6): 966-975 (2005)
[10] Bostater. C., "Airborne multisensor remote sensing systems for subsurface feature detection in littoral zones", SPIE Vol. 8532, pp. 8532081-13 (2012)
[11] Bostater, C., Gimond, M., Campbell, M., "Comparing a hyperspectral Monte-Carlo approach for simulating water surface reflectance signatures based using radiative transfer theory: simulation clear water & Caribbean Sea bottom types", SPIE Vol. 4172, pp. 199-208 (2000)
[12] Smith, R., Baker, K., "Optical properties of the clearest natural waters", Applied Optics, Vol. 20, pp. 177-184 (1984)
[13] Bostater, C., "Modeling water surface reflectance signatures and in-water irradiance profiles in shallow tropical waters influenced by bottom reflectance", IEEE, IGARS 0-7803-3836-7, pp. 881-884 (1997)
[14] Bostater, C., "Specific absorption and backscatter coefficient signatures in southeastern Atlantic coastal waters", SPIE Vol. 3496, pp. 196-200 (1998)
[15] Bostater, C., Klemas, V., "Remote sensing of physical and biological properties of estuaries", IEEE Oceans 1988, IEEE Xplore doi:10.1109/Oceans 1988.23546, pp. 462-466 (1988)
[16] Karp, G., Cell and Molecular Biology, 5th Ed. Wiley (2008)
[17] Bostater, C., Rotkiske, T., "Fluid mud sondes & acoustic methods for coastal dredging", International Society of Offshore and Polar Engineers, ISOPE-I-16-162, Vol. 3, pp. 1561-1567 (2016)

Downloaded From: http://proceedings.spiedigitallibrary.org/ on 04/05/2017 Terms of Use: http://spiedigitallibrary.org/ss/termsofuse.aspx

[18] Bostater, C., Rotkiske, T., ”Moving fluid mud sondes, optical and acoustic sensing methods in support of coastal waterway dredging”, SPIE, Vol. 9623, doi: 10.1117/12.2195829, pp. 96380F1-17 (2015)
[19] Bostater, C., Yang, B “Shallow water surface gravity wave imaging, spectra and their use in shallow water dredging operations, SPIE, Vol. 9240, doi:10.1117/12.2070184, pp. 92400K1-9 (2014)
[20] Bostater, C., “Optimal Band Selection for Hyperspectral Remote Sensing of Aquatic Benthic Features – a Wavelet Filter Window Approach”, SPIE Vol. 6360, pp. 63600L1-10 (2006)

Downloaded From: http://proceedings.spiedigitallibrary.org/ on 04/05/2017 Terms of Use: http://spiedigitallibrary.org/ss/termsofuse.aspx